5284–5296 *Nucleic Acids Research, 2015, Vol. 43, No. 11* *Published online 27 April 2015*
doi: 10.1093/nar/gkv356

Stereochemical control of nucleosome targeting by platinum-intercalator antitumor agents

Eugene Y.D. Chua[1,†], Gabriela E. Davey[1,†], Chee Fei Chin[2,†], Peter Dröge[1], Wee Han Ang[2,*] and Curt A. Davey[1,*]

[1]School of Biological Sciences, Nanyang Technological University, 60 Nanyang Drive, Singapore 637551 and [2]Department of Chemistry, National University of Singapore, 3 Science Drive 3, Singapore 117543

Received February 19, 2015; Revised April 01, 2015; Accepted April 02, 2015

ABSTRACT

Platinum-based anticancer drugs act therapeutically by forming DNA adducts, but suffer from severe toxicity and resistance problems, which have not been overcome in spite of decades of research. And yet defined chromatin targets have generally not been considered in the drug development process. Here we designed novel platinum-intercalator species to target a highly deformed DNA site near the nucleosome center. Between two seemingly similar structural isomers, we find a striking difference in DNA site selectivity *in vitro*, which comes about from stereochemical constraints that limit the reactivity of the *trans* isomer to special DNA sequence elements while still allowing the *cis* isomer to efficiently form adducts at internal sites in the nucleosome core. This gives the potential for controlling nucleosome site targeting *in vivo*, which would engender sensitivity to epigenetic distinctions and in particular cell type/status-dependent differences in nucleosome positioning. Moreover, while both compounds yield very similar DNA-adduct structures and display antitumor cell activity rivalling that of cisplatin, the *cis* isomer, relative to the *trans*, has a much more rapid cytotoxic effect and distinct impact on cell function. The novel stereochemical principles for controlling DNA site selectivity we discovered could aid in the design of improved site discriminating agents.

INTRODUCTION

The 'classic' platinum drugs, such as the prototypic cisplatin, achieve their therapeutic efficacy by taking advantage of certain vulnerabilities of cancer cells through forming DNA lesions, which interfere with genomic activities and ultimately trigger apoptosis (1,2). The underlying problem is that these simple small molecules are associated with severe toxicity and intrinsic or acquired resistance effects (3,4). Thus, one possibility is that rationally designed platinum derivatives could avoid binding to counterproductive sites while hitting one or more therapeutic targets. However, in spite of their widespread application for decades in the treatment of specific cancers and the execution of many thousands of clinical and chemical studies, little progress has been made in assessing the therapeutic potential of targeting selective genomic sites.

The majority of cellular DNA is wrapped by histone proteins into nucleosomes, rendering these fundamental repeating units of chromatin an important therapeutic target (5). In fact, recent studies are uncovering profound epigenetic differences between normal and tumor cells, corresponding to distinctions in chromatin structure and chemical composition (6–8). This suggests there are many potential cancer-specific nucleosome targets in the genome, and it has also become clear there are a number of genes critical for cancer cell survival that are relatively dispensable to normal cells (9,10). Considering moreover that platinum drugs may exert their antitumor effects primarily by inhibiting transcription (2) and that the DNA damage response is altered in transformed—and in particular drug-resistant—cells (8), differential adduct distribution throughout the genome could result in highly distinct cellular impact. Indeed, histone octamer-associated DNA, relative to naked DNA, inhibits the nucleotide excision repair of cisplatin adducts *in vitro* (11), suggesting that lesions residing within the nucleosome core may be more efficacious. Therefore, one idea is to find compounds capable of binding to specific nucleosomes or defined sites within nucleosomes, which could enable targeting genomic weak points of cancer cells.

We earlier found that the 'sugar-clamp' DNA-binding histone motif situated 1.5 double helical turns from the nucleosome center (SHL ± 1.5) can induce an extraordinary kink distortion in certain DNA sequences (12,13). This site on the nucleosome is by no coincidence a favored location for

*To whom correspondence should be addressed. Tel: +65 6592 1549; Fax: +65 6791 3856; Email: davey@ntu.edu.sg
Correspondence may also be addressed to Wee Han Ang. Tel: +65 6516 5131; Fax: +65 6779 1691; Email: chmawh@nus.edu.sg
†These authors contributed equally to the paper as first authors.

retroviral genome integration by the HIV integrase, which has a preference for highly distorted substrate (14,15). In fact, we found that the extreme kinking into the minor groove can also predispose small molecule intercalation at the unstacked major groove edge, which creates a hotspot for DNA alkylation in the nucleosome by an intercalating epoxide antitumor species (16). We had taken this as a lead to design more stable and selective therapeutic candidates by replacing the epoxide group with a platinum functionality.

Here we conducted structural and functional analysis of two novel platinum-intercalator compounds: *cis*-chloro[1,2,3-diethylenetriamino-2-*N*-(3-propyl)-1,8-naphthalimide]platinum(II) chloride (**cisPtNAP**) and *trans*-chloro[1,2,3-diethylenetriamino-1-*N*-(3-propyl)-1,8-naphthalimide]platinum(II) chloride (**trPtNAP**; Figure 1). We found that one of these structural isomers forms DNA adducts at defined, internal locations within the nucleosome core, while the other efficiently forms adducts only at the most flexible and conformationally unconstrained sites of DNA. Therefore, these compounds are unique in displaying a significant level of DNA site discrimination, unlike existing platinum drugs (17,18). Moreover, the two compounds show antitumor cell activity that rivals that of cisplatin, and this is achieved without the capacity to form cross-links.

MATERIALS AND METHODS

Synthesis of cisPtNAP and trPtNAP

The synthesis of the two PtNAPs are summarized in Figure 1 and outlined in Scheme S1. Naphthalimide precursors **1** and **2** were prepared in accordance to published protocols (19). Ligand **3** was obtained by reacting **2** with neat diethylenetriamine at 70° C for 2 h. Precursor **4** was synthesized by refluxing boc-protected diethylenetriamine with **2** in 1:1 v/v MeCN/$CHCl_3$ for 2 d. $CHCl_3$ was added to the reaction medium due to the poor solubility of **2** in MeCN. Precursor **4** was purified by flash column chromatography over silica and deprotected using concentrated HCl to yield ligand **5**. TrPtNAP was obtained by refluxing excess ligand **5** and *cis*-$PtCl_2(DMSO)_2$ in MeOH. The reaction mixture was evaporated to dryness and washed sequentially with diethyl ether and CH_2Cl_2 to remove unreacted ligand **5**. CisPtNAP was synthesized from ligand **3** using a similar approach. The detailed synthetic procedures are given in the following paragraphs.

N-*(3-hydroxylpropyl)naphthalimide, 1.* 1,8-naphthalic anhydride (2.50 g, 0.013 mol) was added to 3-amino-1-propanol (1.0 ml, 0.013 mol) in EtOH (20 ml) and refluxed for 1.5 h. The reaction mixture was concentrated under reduced pressure and subsequently cooled at 4°C. The resulting precipitate was filtered and the residue washed with cold EtOH to afford **2** as a pale brown solid (2.59g, 78%). ^{1}H NMR ($CDCl_3$, 300 MHz): δ 8.62 (d, 2 H, Ar-H), 8.59 (d, 2H, Ar-H), 7.76 (dd, 2H Ar-H), 4.35 (t, 2H, CCH_2O), 3.59 (t, 2H, NCH_2C), 3.12 (br, 1H, OH), 2.01 (m, 2H, CCH_2C).

N-*(3-bromopropyl)naphthalimide, 2.* PBr_3 (0.8 ml, 8.51 mmol) was added to a stirred suspension of **1** (1 g, 4.149 mmol) in MeCN (5 ml). The reaction mixture was stirred at room temperature for 20 m, and subsequently heated at 75° C for 1.5 h. The reaction mixture was cooled, added to ice water (15 ml) and extracted with $CHCl_3$ (3 × 50 ml). The extract was washed with saturated $NaHCO_3$ (10 ml), followed by water (3 × 50 ml), and the purity of the product was monitored by TLC. The solvent was evaporated under reduced pressure to afford **3** as a pale yellow solid (1.03 g, 78%). ^{1}H NMR ($CDCl_3$, 300 MHz): δ 8.60 (d, 2 H, Ar-H), 8.22 (d, 2H, Ar-H), 7.76 (t, 2H Ar-H), 4.33 (t, 2H, CCH_2O), 3.50 (t, 2H, NCH_2C), 2.34 (m, 2H, CCH_2C).

Ligand 3. Compound **2** (500 mg, 1.57 mmol) was added to a stirring mixture of neat diethylenetriamine (2 ml, 18.5 mmol) and triethylamine (0.5 ml, 3.59 mmol) and heated at 70° C for 2 h. The reaction mixture was cooled and added to excess ether (50 ml). The mixture was filtered and the filtrate was evaporated under reduced pressure. The residue was subsequently dissolved in water (7 ml), and the product was extracted with $CHCl_3$ (3 × 20 ml) to afford ligand **3** as a viscous yellow liquid (444 mg, 83%). ^{1}H NMR ($CDCl_3$, 300 MHz): δ 8.21 (d, 2H, Ar-H), 7.86 (d, 2H, Ar-H), 7.41 (t, 2H, Ar-H), 2.41 – 2.58 (m, 12H, NCH_2), 1.69 (m, 2H, CCH_2C), NH resonances were not assigned.

Ligand 5. Boc-protected diethylenetriamine (0.352 g, 1.16 mmol) was stirred in MeCN/$CHCl_3$ (20 ml, 1:1 v/v). Triethylamine (0.485 ml, 3.48 mmol) was added to the reaction mixture, which was stirred at room temperature for 30 m. Compound **2** (0.369g, 1.16 mmol) was then added and the reaction was refluxed for 2 d. The solvent was removed and was separated by flash column chromatography over silica to yield **4** as a colorless liquid (0.190 g, 30%). Compound **4** was directly deprotected in 4 M HCl/dioxane (4 ml) at 60°C for 12 h. The white precipitate was filtered and washed with diethyl ether (3x 5 ml) to afford ligand **5** as a **5**·3HCl salt. ^{1}H NMR of **4** ($CDCl_3$, 300 MHz): δ 8.52 (d, 2H, Ar-H), 8.15 (d, 2H, Ar-H), 7.69 (t, 2H, Ar-H), 5.30 (br, 2H, NH), 4.16 (t, 2H, NCH_2), 3.15 (d, 4H, $NHCH_2$), 2.53 (m, 6H, NCH_2), 1.85 (m, 2H, CCH_2C), 1.38 (s, 18H, CCH_3). ^{1}H NMR of **5**·3HCl (D_2O, 300 MHz): δ 7.69 (d, 4H, Ar-H), 7.22 (t, 2H, Ar-H), 3.72 (t, 2H, NCH_2), 3.42 – 3.61 (m, 8H, NCH_2CH_2N), 3.36 (m, 2H, NCH_2), 1.95 (m, 2H, CCH_2C); $^{13}C\{^1H\}$ of **5**·3HClNMR (D_2O, 75.5 MHz): 164.0 (s, CO), 134.9, 130.9, 129.8, 126.6, 125.5, 119.1 (s, Ar-H), 52.0 (s, NC), 49.7 (s, NC), 36.9 (s, NC), 33.5 (s, NC), 22.0 (s, CH_2).

TrPtNAP. Ligand **5**·3HCl (40 mg, 0.118 mmol) was neutralized with K_2CO_3 (171 mg, 1.24 mmol) in DMSO:DMF:water (10 ml, 1:1:1 v/v) at room temperature for 12 h. The reaction mixture was extracted with CH_2Cl_2 (3 × 10 ml) and dried over Na_2SO_4. The solvent was removed and **5** was dissolved in MeOH (8 ml). *Cis*-$PtCl_2(DMSO)_2$ (40 mg, 0.095 mmol) was added, and the solution mixture was refluxed for 2 h. The solvent was removed and residue was washed with diethyl ether (3 × 20 ml) and cold CH_2Cl_2 (1 × 10 ml) to afford trPtNAP as a light brown solid (41 mg, 76%). ^{1}H NMR (DMSO, 500 MHz): 8.50 (d, 4H, Ar-H), 7.88 (t, 2H, Ar-H), 5.34 – 5.69

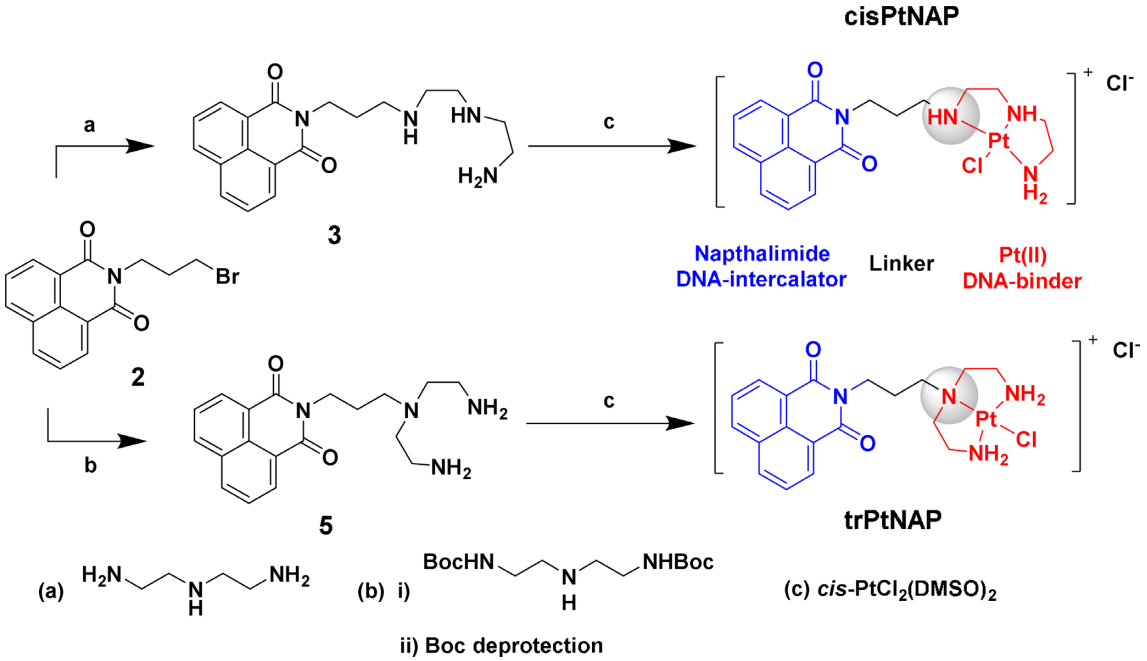

Figure 1. Design and synthesis of the platinum-intercalator agents.

(br, NH), 4.11 (t, 2H, NCH_2), 3.47 (t, 2H, NCH_2), 3.12 (d, 4H, NCH_2), 2.96 (d, 2H, NCH_2), 2.84 (d, 2H, NCH_2), 1.97 (m, 2H, CCH_2C). $^{13}C\{^1H\}$ NMR (DMSO, 125.8 MHz): 163.6 (s, CO), 134.3, 131.3, 130.7, 127.4, 127.2, 122.0 (s, Ar-C) 60.8 (s, NC), 52.2 (s, NC), 47.8 (s, NC), 37.3 (s, NC), 21.0 (s, CH_2). ESI (MS) m/z = 571 $[M]^+$. Anal. Calcd. for trPtNAP, $C_{19}H_{24}Cl_2N_4O_2Pt$: C, 37.63; H, 3.99; N, 9.24. Found: C, 37.37; H, 3.70; N, 9.15.

CisPtNAP. Ligand **3** (220 mg, 0.647 mmol) was dissolved in MeOH (10 ml) and *cis*-$PtCl_2(DMSO)_2$ (200 mg, 0.475 mmol) was added. The reaction was refluxed for 2 h and the solvent was subsequently removed. The residue was washed with diethyl ether (3 × 40 ml) and cold MeOH (1 × 10 ml) to afford cisPtNAP as a light yellow solid (230 mg, 80%). ^1H NMR (DMSO, 500 MHz): 8.47 (m, 4H, Ar-H), 7.87 (t, 2H, Ar-H), 5.46 – 6.67 (br, NH), 2.00 – 4.07 (br, 14H, NCH_2/CCH_2C), 1 set of NCH_2 peaks overlap with H_2O peak. $^{13}C\{^1H\}$ NMR (DMSO, 125.8 MHz): 163.5 (s, CO), 134.3, 131.3, 130.7, 127.4, 127.2, 122.0 (s, Ar-C), 57.3 (s, NC), 54.3 (s, NC), 53.1 (s, NC), 50.4 (s, NC), 49.8 (s, NC), 48.6 (s, NC), 37.1 (s, NC), 25.9 (s, CH_2). ESI (MS) m/z = 571 $[M]^+$. Anal. Calcd. for cisPtNAP, $C_{19}H_{24}Cl_2N_4O_2Pt$: C, 37.63; H, 3.99; N, 9.24. Found: C, 37.51; H, 4.36; N, 9.00.

Determination of cell growth inhibition parameters

Human ovarian carcinoma cell lines, A2780 and cisplatin-resistant A2780 (crA2780), were purchased from the Health Protection Agency Culture Collections (HPACC, Salisbury, UK) and grown at 37°C and 5% CO_2 in RPMI 1640 medium containing 10% fetal calf serum with 2 mM glutamine, 100 units ml^{-1} penicillin and 100 μg ml^{-1} streptomycin. The crA2780 cells were additionally treated with 1 μM cisplatin for every 2–3 passages to maintain resistance. HaCaT cells (non-tumorigenic human keratinocytes; ATCC, USA) were generously provided by Andrew N.S. Tan and grown at 37°C and 5% CO_2 in DMEM medium containing 10% fetal calf serum with 2 mM glutamine, 1 mM pyruvate, 100 units ml^{-1} penicillin and 100 μg ml^{-1} streptomycin. Cisplatin was purchased from Sigma-Aldrich, USA (P4394–250MG).

To measure the cytotoxicity from exposure to different agents, cells were seeded in 96-well plates (5000 cells per well) and grown for 24 h. Stock solutions were prepared by dissolving cisplatin in complete medium, and by initially dissolving trPtNAP, cisPtNAP and naphthalimide in DMSO followed by subsequent addition into complete medium. These medium stocks were then subjected to serial dilutions and added to the cells at various concentrations. The DMSO concentration in the medium never exceeded 0.5% and was set constant within a given assay, including control cells.

Following a 72 h incubation, media were aspirated and 100 μl of 10% 3-(4,5-Dimethylthiazol-2-yl)-2,5-diphenyltetrazolium bromide (TOX1–1KT; MTT kit, Sigma-Aldrich, USA) in RPMI or DMEM complete medium was added to cells, which were incubated for 3 h at 37°C. Subsequently, 100 μl of solubilisation buffer was added to each well with vigorous pipetting in order to dissolve formazan. The resulting optical density was measured at 570 and 690 nm using a multi-well plate reader (Infinite M200 PRO, Magellan data analysis software, TECAN, Switzerland). The ratios of surviving cells were calculated by comparing to the untreated samples, and the IC_{50} was derived based on at least three data sets (see Table 1).

Table 1. Cell growth inhibition parameters

	A2780[a]	crA2780[a]	Resistance[b]	Non-tumor[a,d]
Cisplatin	1.00 ± 0.05[c]	14.0 ± 0.3[c]	14.0	3.58 ± 0.87
cisPtNAP	0.25 ± 0.02	0.48 ± 0.02	1.9	18.4 ± 2.2
24 h	3.58 ± 0.33			
trPtNAP	0.18 ± 0.05	0.32 ± 0.08	1.8	26.8 ± 0.8
24 h	>40.0			
Naphthalimide	55.3 ± 3.6	96.3 ± 9.5	1.7	

[a]IC_{50}, μM; based on 72 h treatment, unless indicated otherwise.
[b]crA2780:A2780 IC_{50} value ratio (fold resistance).
[c]From (21).
[d]HaCaT (non-tumorigenic human keratinocytes).
Mean ± SD, $n = 3$.

Genomic DNA adduct quantification

Isolation of genomic DNA was carried out using a GenElute Mammalian Genomic DNA Miniprep Kit (G1N70; Sigma Aldrich, USA). A2780 cells were maintained in culture as described above. For the measurements in Table 2, cells were grown in 60 mm plates to approximately 90% confluency before being incubated with 18 μM trPtNAP, 25 μM cisPtNAP or 100 μM cisplatin for 18 h at 37°C. The amount of DNA was quantified by UV absorption measurements at 260 nm and subjected to atomic absorption spectroscopic analysis to measure platinum content. Determination of platinum levels on DNA was conducted by pipetting 20 μl of sample into the reaction chamber of a Hitachi Z-2000 Polarized Zeeman Atomic Absorption Spectrophotometer in graphite furnace mode.

Cellular death and cell cycle analyses

Cells were seeded into 35 mm-wells, incubated overnight, and the following day 2 μM cisPtNAP or trPtNAP were added into triplicate samples for 24-h incubation. Subsequently, the medium containing compound was removed and replaced with fresh medium. The cells were collected for analysis immediately (day 1) and subsequent to further 24-h (day 2) and 48-h (day 3) incubations in compound-free media.

Extent of apoptosis/necrosis was assessed utilizing an Annexin-V-FLUOS staining kit (11988549001; Roche Diagnostics, Germany). Floating cells as well as attached cells were collected, washed in PBS and stained with Annexin V and Propidium Iodide (PI). Cells were then incubated for 15 min in the dark and analyzed on an LSR II flow cytometer (BD FACSDiva software, BD Biosciences).

For the cell cycle analysis, cells were rinsed in PBS, trypsinized, pelleted and washed before they were added in a drop-wise manner into 70% ethanol. After overnight-incubation, cells were washed in PBS and incubated with DAPI dihydrochloride (3 μM, Life Technologies) for 15 min in the dark before analyzing on an LSR II flow cytometer (BD FACSDiva software, BD Biosciences).

Analysis of cellular data was based on three independent replicates of each experiment. Graphic plots were generated with Excel (Microsoft Corporation). Mahalanobis multivariate analysis (20,21) was carried out using Xlstat (version 2013.1.01; Addinsoft Corporation).

DNA footprinting analysis

Exonuclease III footprinting experiments for obtaining PtNAP adduct formation profiles, based on digest (3′ to 5′ direction) termination at DNA lesion sites, were conducted in a similar fashion as described previously for platinum adduct mapping (17,18). 1 mM stock solutions of trPtNAP and cisPtNAP were prepared by dissolving agent in DMSO. 2.5 μM naked DNA or NCP in a buffer of 20 mM K-cacodylate (pH 6.0) were incubated at room temperature for 24 h in the dark with a 10-, 20- or 50-fold molar excess for trPtNAP, and a 5-, 10- or 50-fold molar excess for cisPtNAP. An equal volume of 4 M NaCl was then added to each reaction, and the samples heated at 55°C for 1 h to dissociate DNA from histones. To precipitate the histones, 0.5 volumes of phenol and CIA (24:1 chloroform:isoamyl alcohol) were added to the mixture, which was then vortexed for 1 m. The phases were separated by centrifugation at 14 500 rpm for 3 m at room temperature, and the DNA was ethanol-precipitated from the aqueous phase and redissolved in a buffer of 10 mM Tris (pH 7.5) and 0.1 mM EDTA (pH 8.0) to the desired concentration.

DNA samples were 5′ end-labeled by T4 polynucleotide kinase in reactions containing 1.5 μM DNA, 0.5 μCi μl^{-1} γ^{32}P-ATP, 0.5 units μl^{-1} T4 polynucleotide kinase and 1.5X polynucleotide kinase buffer (New England Biolabs, USA), incubated at 37°C for 60 m. Samples were then purified by centrifugation at 800 g for 3 m with DyeEx 2.0 Spin Kits (Qiagen, Germany). Exonuclease III digestion was typically conducted in 50 μl reactions containing 0.15 μM DNA, 5 units μl^{-1} Exonuclease III, and 1X NEBuffer 1 (New England Biolabs, USA) at 37°C for 60 m. The digestion was stopped by adding 0.5 volumes of a solution of 0.9 M sodium acetate and 0.09 M EDTA, and 4 volumes of cold 100% ethanol, with a 10 m incubation on ice. The samples were centrifuged at 12 000 rpm for 5 m at room temperature, and the pellets were washed with cold 70% ethanol to remove excess salt. The precipitated DNA fragments were resuspended in 200 μl of 1 M thiourea and incubated at 58°C overnight to deplatinate the DNA. Upon completion of deplatination, 0.1 volumes of 3 M sodium acetate and 3 volumes of cold 100% ethanol were added, and the samples incubated for 10 m on ice to precipitate the DNA. The samples were centrifuged at 12 000 rpm for 5 m at room temperature, and the pellets were washed with cold 70% ethanol to remove any crystalline thiourea. Following a final round of centrifugation at 12 000 rpm for 5 m, the precipitated DNA

Table 2. Platinum adduct levels on genomic DNA

adducts	cisPtNAP	trPtNAP	Cisplatin
Per 10^6 bp[a]	787 ± 144	557 ± 110	1235 ± 50
Relative (μM^{-1})[b]	31.5	30.9	12.3

[a]Platinum atoms per 10^6 base pairs (bp); Agent concentrations used in cell treatments, 25 μM cisPtNAP, 18 μM trPtNAP, 100 μM cisplatin.
[b]Platinum atoms per 10^6 bp per μM of compound used in cell treatment.
Mean ± SD, $n = 3$.

fragments were dissolved in 1X denaturing DNA loading dye (95% v/v formamide, 0.025% w/v Bromophenol blue, 0.025% w/v Xylene cyanol FF, 0.5 mM EDTA), heated at 95°C for 3 m, immediately chilled on ice, and then analyzed on 9% denaturing PAGE.

Maxam-Gilbert purine sequencing standards (22) were prepared by 5′ end-labeling unreacted DNA samples with T4 polynucleotide kinase as described above. To the labeled samples, formic acid was added to a final concentration of 57% and allowed to react for 4–6 m at room temperature. The reaction was quenched by adding 6 volumes of 0.3 M sodium acetate, 0.1 M EDTA and 25 μg ml^{-1} RNA, and the DNA was precipitated immediately by addition of 3 volumes of cold 100% ethanol. After 10 m incubation on ice, the samples were centrifuged at 12 000 rpm for 5 m, and the pellets were washed with cold 70% ethanol. The pellets were then dissolved in 200 μl 10% (v/v) piperidine with 50 mM EDTA and heated at 99°C for 45 m to cause strand cleavage at formic acid-modified purine bases. The reaction was stopped by ethanol precipitation and the standards used in the analysis described above.

Denaturing polyacrylamide gel electrophoresis

9% denaturing polyacrylamide gels were cast in 42.5 cm x 21 cm x 0.75 mm gel plates. The gel was pre-run at 60 W at room temperature until the gel temperature reached 55°C. Labeled DNA samples with approximately equal radioactive counts in 1X denaturing DNA loading dye were heated at 100°C for 5 m and then loaded into each well, and the gel run at 55 W for 2 or 3 h at room temperature in 0.5X TBE buffer (44.5 mM Tris, 44.5 mM Boric acid, 1 mM EDTA). The gel was harvested onto Whatman filter paper, fixed with 0.5X TBE, 5% methanol and 5% acetic acid, and dried at 65°C for 2 h by using a Slab Gel Drier Model GD2000. DNA bands were visualized by exposing the dried gel to Imaging Screen-K for 12–72 h, and the screen was scanned by using a Molecular Imager FX machine. Quantity One (Bio-Rad Laboratories) was used to quantify the intensity of gel bands.

Crystallographic analysis of treated nucleosome core particle

NCP crystals were produced and stabilized in harvest buffer (37 mM $MnCl_2$, 40 mM KCl, 20 mM K-cacodylate [pH 6.0], 24% 2-methyl-2,4-pentanediol and 2% trehalose) as previously described (23). The 37 mM $MnCl_2$ buffer component was subsequently eliminated by gradual replacement with 10 mM $MgSO_4$ followed by thorough rinsing of crystals with the $MgSO_4$-containing buffer to remove any residual $MnCl_2$ (24). PtNAP agents were dissolved in the $MgSO_4$-containing buffer at varying concentrations, which was used to soak the crystals for various incubation times at room temperature. The NCP-PtNAP crystal structures reported here stem from a 24-h incubation with 0.1 mM trPtNAP and a 23-h incubation with 0.25 mM cisPtNAP.

Single crystal X-ray diffraction data were recorded, with crystals mounted directly into the cryocooling N_2 gas stream set at −175°C (21), at beam line X06DA of the Swiss Light Source (Paul Scherrer Institute, Villigen, Switzerland) using a Mar225 CCD detector and an X-ray wavelength of 1.07 Å (platinum absorption edge). Data were processed with MOSFLM (25) and SCALA from the CCP4 package (26).

Native NCP models (18,23,27) were used for initial structure solution by molecular replacement. Structural refinement and model building were carried out with routines from the CCP4 suite (26). Models for cisPtNAP and trPtNAP were built by combining crystallographic data files of *N*-(2,3-epoxypropyl)-1,8-naphthalimide (CCDC deposition number 756223) (16) and a platinum-diethylenetriamine complex (CCDC deposition number 663059) (28). Data collection and structure refinement statistics are given in Supplementary Table S1. Dinucleotide step conformational parameters were obtained by using 3DNA (29,30). Graphic figures were prepared with PyMOL (DeLano Scientific LLC, San Carlos, CA, USA).

RESULTS

Design of nucleosome-targeting platinum-intercalator agents

Our design of a nucleosome-targeting agent consists of a DNA intercalator linked to a Pt-amine motif capable of covalent DNA-binding (Figure 1). The Pt(diethylenetriamine) functional group was installed as the Pt-amine motif for three reasons. Firstly, the diethylenetriamine ligand could be readily attached to the DNA intercalator via classical substitution at either a terminal or the central nitrogen atom. Secondly, the tridentate ligand could effectively occupy three coordination sites around the square-planar Pt(II) complex to yield selectively a stable and monofunctional DNA-binding motif. Thirdly, the Pt-amine group could interact favorably with guanine via H-bonding with the exocyclic O6 atom, directing Pt toward the nucleophilic N7 atom, conferring some degree of selectivity over other nucleobases. A propylene linker was installed to provide a separation of up to 5 Å between the napthalimide intercalator and Pt-amine groups, and to confer structural flexibility to accommodate the anticipated two-fold DNA interaction. The selection of the napthalimide intercalator was based on our earlier report demonstrating its favorable insertion into the ‘open’ major groove face of extremely kinked DNA sites (16).

Toward that end, we prepared cisPtNAP and trPtNAP as summarized in Figure 1. *N*-(3-bromopropyl)naphthalimide **2** was prepared in 2 steps from 1,8-napthalic anhydride. Ligand **3**, comprising the propyl-napthalimide motif linked terminally to diethylenetriamine, was synthesized directly by reacting **2** with neat diethylenetriamine. Treatment of **3** with *cis*-$PtCl_2(DMSO)_2$ afforded the desired cisPtNAP complex with the Pt-binding group oriented *cis*- to the napthalimide intercalator, from the perspective of their expected interaction with kinked DNA. Ligand **5** was prepared in 2 steps from **2** using terminally boc-protected diethylenetriamine and boc deprotection in HCl/dioxane. Similarly, treatment with *cis*-$PtCl_2(DMSO)_2$ yielded trPtNAP, which contained the Pt-binding group oriented *trans*- to napthalimide. Details of the synthesis and chemical analysis of the two compounds are described above and in the Supplementary Data (Scheme S1, Supplementary Figures S1–S4).

Potent and specific activity against tumor cells

We conducted cell growth inhibition assays for the two platinum-intercalator species, cisPtNAP and trPtNAP, and compared with the activity of cisplatin (Table 1). For the commonly used 3-day agent exposure assays, we found that cisPtNAP and trPtNAP are approximately 4-fold and 5-fold, respectively, more cytotoxic than cisplatin to human ovarian (A2780) cancer cells. To confirm that these low IC_{50} values, 0.25 μM and 0.18 μM respectively for cisPtNAP and trPtNAP, were not largely due to the intercalator activity itself, we tested the cell growth inhibitory capacity of 1,8-naphthalimide. Indeed, the naphthalimide functionality alone yields a much higher IC_{50} value (55.3 μM), which corresponds to respectively 221-fold and 307-fold lower cytotoxicity than cisPtNAP and trPtNAP.

Alongside the A2780 cell assays, we also tested the activity of cisPtNAP and trPtNAP on inhibiting the growth of a cisplatin-resistant A2780 (crA2780) cell line (31). The crA2780 cells are 14-fold resistant to cisplatin (IC_{50} = 14 μM) relative to the A2780 cells. However, the cytotoxicity of cisPtNAP (IC_{50} = 0.48 μM) and trPtNAP (IC_{50} = 0.32 μM) to these resistant cells is only 1.9-fold and 1.8-fold, respectively, below that observed for the A2780 cells. This corresponds to a basal level of cross-resistance, common to DNA damaging agents completely unrelated to cisplatin (21,31).

In order to assess the therapeutic potential of cisPtNAP and trPtNAP in terms of selective activity against tumor cells, we also tested impact on a model for healthy tissue, HaCaT cells, which are a non-tumorigenic human keratinocyte line that is well suited for tissue culture. Interestingly, cisplatin is still appreciably toxic to the HaCaT cells, with a 3.6 μM IC_{50}, which corresponds to an only 3.6-fold increase over that for the A2780 cells. On the other hand, the respective HaCaT IC_{50} values for cisPtNAP and trPtNAP, 18.4 μM and 26.8 μM, are much higher than for the A2780 cells, corresponding to diminished cytotoxicity on the order of 74-fold and 149-fold respectively.

Proficient accumulation of adducts on cellular DNA

Given the chemical nature of cisPtNAP and trPtNAP, one would assume their very high cytotoxicity to tumor cells is stemming from DNA adducts. To establish DNA adduct formation potential, we treated cells with agent at concentrations proportional to their 3-day IC_{50} values for 18 h, isolated the genomic DNA and quantified platinum adduct levels (Table 2). This analysis showed that cisPtNAP and trPtNAP form similar levels of adducts, namely approximately 8 and 6 adducts, respectively, per 10^4 base pairs (bp). This corresponds to about one-half the adduct levels found for analogous treatment with cisplatin, which yields ∼12 adducts per 10^4 bp. On the other hand, relative to the agent concentration used in the cell treatment, cisPtNAP and trPtNAP yield almost identical adduct levels, ∼31 adducts per 10^6 bp per μM, which is in fact a genomic DNA adduct formation activity that is roughly 2.5-fold greater than that of cisplatin (∼12 adducts per 10^6 bp per μM).

Isomer-dependent DNA site selectivity

With the very similar activity of cisPtNAP and trPtNAP observed from the cellular cytotoxicity and genomic DNA adduct formation assays described above, it would seem to follow that the two compounds have similar DNA site selectivity. However, DNA footprinting analysis of agent-treated nucleosome core particle (NCP) and the corresponding naked DNA show that this is not the case (Figures 2 and 3, Supplementary Figure S5). For this method, as well as for the X-ray crystallographic analysis, a palindromic 145 bp DNA fragment was utilized and nucleosome core assembled with recombinant histones using established protocols (12,23,24,32).

In the footprinting analysis, although both isomers show a clear discrimination to form adducts at only guanine nucleotides, they display highly distinct preferences for specific DNA sequence elements—that is the sequence context of the guanine sites. Moreover, the site discrimination seen toward the nucleosomal substrate is dramatically different, with trPtNAP forming substantial adducts only at the guanine nucleotides nearest the DNA termini of the nucleosome core. In fact, this agent has a striking preference for a palindromic CTGCAG element (SHL ± 5.5/6), where it efficiently forms adduct at nucleotide −58 (underlined) on both the naked DNA and NCP substrates. The selectivity for this particular sequence element is so pronounced that it is the sole site of significant adduct formation at low trPtNAP concentrations.

In contrast to the selectively of trPtNAP toward specific DNA sequence elements, cisPtNAP avidly forms adducts at internal nucleosomal sites and in particular at the location of superkinking at SHL ± 1.5. Thus, cisPtNAP is effective at targeting the highly deformed DNA site in the nucleosome for which it was designed, whereas adduct formation by trPtNAP at this location is barely detectable in the solution state.

Stereochemical reactivity control in platinum-intercalator species

In order to understand the basis for the profound difference in site selectivity displayed by cisPtNAP and trPtNAP, we conducted X-ray crystallographic experiments in which we derivatized NCP crystals that are composed of the same

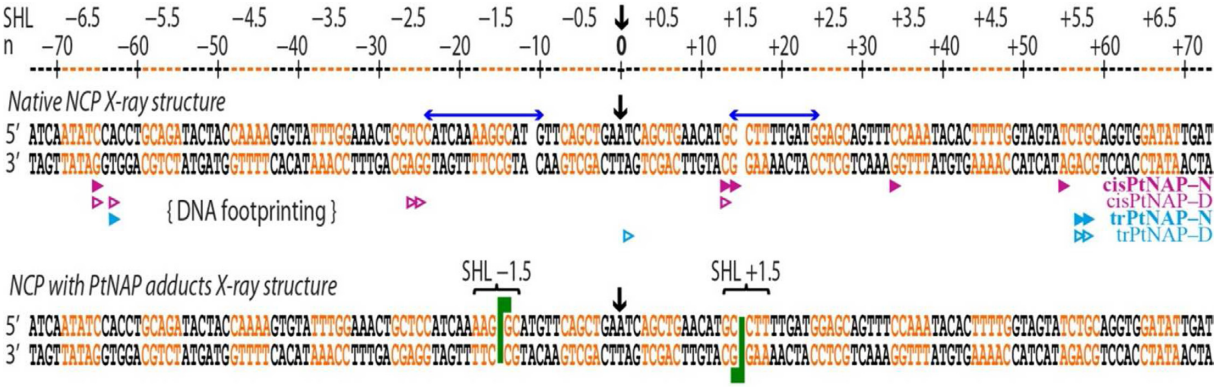

Figure 2. DNA sequence, context and platinum-intercalator site selectivity. Preferences of cisPtNAP and trPtNAP adduct formation with respect to double helix state, structure and sequence (native NCP structure, upper; treated NCP structure, lower; PtNAP adducts in structure, green). Orange and black lettering for the DNA sequence designate regions where the minor as opposed to the major groove, respectively, face inward toward the histone octamer in the NCP. In the native NCP, locations of DNA stretching around SHL ± 2 (blue arrows) result in severe kinks into the major groove (left half, SHL −1) or into the minor groove (right half, SHL +1.5) and a shift in the histone-DNA register, depicted as a gap in the sequence. The footprinting analysis of PtNAP-treated naked DNA (D) and nucleosomal DNA (N), shown in Figure 3, is summarized with exonuclease stop sites depicted as arrowheads, adjacent to the terminal 3′ nucleotide, pointing toward the platinum adduct.

DNA fragment used in the footprinting studies. We carried out many trials to find the best compromise between adduct occupancy and resolution, as longer duration and higher concentration treatments yield progressively higher site occupancy albeit correspondingly lead to greater disordering of the crystals and thus lower resolution data.

We determined treatment strategies that allowed us to acquire 2.6 Å and 2.45 Å resolution data sets for cisPtNAP and trPtNAP, respectively, with which we could build accurate atomic models for DNA adducts formed by each isomer (Supplementary Table S1). For both compounds, we observe adducts only at the locations of extreme DNA kinking in both symmetry-related halves of the nucleosome (SHL −1.5 and +1.5; Figures 2 and 4), with one exception relating to cisPtNAP, which is observed to also associate with one of the NCP DNA termini. It is not clear whether this corresponds to an adducted state, but in any case it is an artifact of (non-physiological) DNA termini, which loosely stack between neighboring NCPs in the crystal and thus promote intercalation of the naphthalimide group.

To pinpoint the locations of the platinum atoms and to detect adduct sites also with low occupancy, we collected diffraction data at the X-ray absorption edge for platinum. The anomalous difference electron density maps calculated with these data show that for cisPtNAP, there are actually three distinct platinum atom locations around the GG dinucleotide element of SHL ± 1.5 (Figure 4, Supplementary Figures S6 and S7). The major adduct configuration of these three corresponds to platinum coordination to the 3′ guanine N7 group and is sufficiently populated to allow construction of an atomic model. The naphthalimide group is nearly fully intercalated within the GG step, and the cisPtNAP amine group connecting the naphthalimide group forms a hydrogen bond with the O6 atom of the coordinating guanine base. The two additional, minor, platinum atom configurations correspond to alternate coordination to the 5′ guanine base of the GG element and what appears to be an alternate intercalative mode associated with a distinct stretching configuration of the double helix. We note that cisPtNAP contains a chiral center at the linker-connecting nitrogen group, which is expected to exchange with solvent to yield a racemic mixture of both protonation state enantiomers. What we have modeled in the adduct structures is the configuration that is most consistent with the electron density, which also coincides with allowing hydrogen bonding to the O6 atom of the platinum-bound guanine base.

For trPtNAP, there are two distinct configurations in the crystal that are sufficiently populated to allow atomic modeling (Figures 4 and 5, Supplementary Figures S6 and S8). One of these is observed clearly at both symmetry-related sites (SHL −1.5 and +1.5) and entails adduct formation at the same site as for cisPtNAP. The trPtNAP and cisPtNAP adduct structures are similar, however the different configuration of linkage between the intercalator and platinum head groups results in differential orientation of the naphthalimide plane and triamine ligand. The triamine group in the trPtNAP adducts is oriented with an inclination that allows for hydrogen bonding with both the 5′ phosphate group and guanine O6 atoms on the opposing side. The other binding configuration of trPtNAP, seen with sufficient clarity to allow model building only for SHL +1.5, corresponds to a mode of intercalation in which the platinum atom is not coordinated to the DNA (Figure 5). The naphthalimide group resides within the GG bp step element as in the case for the adducts, but the platinum head group is localized instead adjacent to the 5′ guanine with the platinum atom situated axially ∼3.7 Å from the O6 atom. Although this non-adductive binding mode must be largely promoted by the hydrophobic interactions of intercalation, it seems to be additionally stabilized by hydrogen bonding between one of the amine ligands and the N7 group of the adjacent adenine to the 5′ side. This non-adducted binding mode is also apparent, albeit with poor clarity either because of structural disorder or low occupancy, in the symmetry-related site at SHL −1.5 (Supplementary Figure S8).

The adducts formed by cisPtNAP and trPtNAP at the locations of superkinking are seen to result in nearly identi-

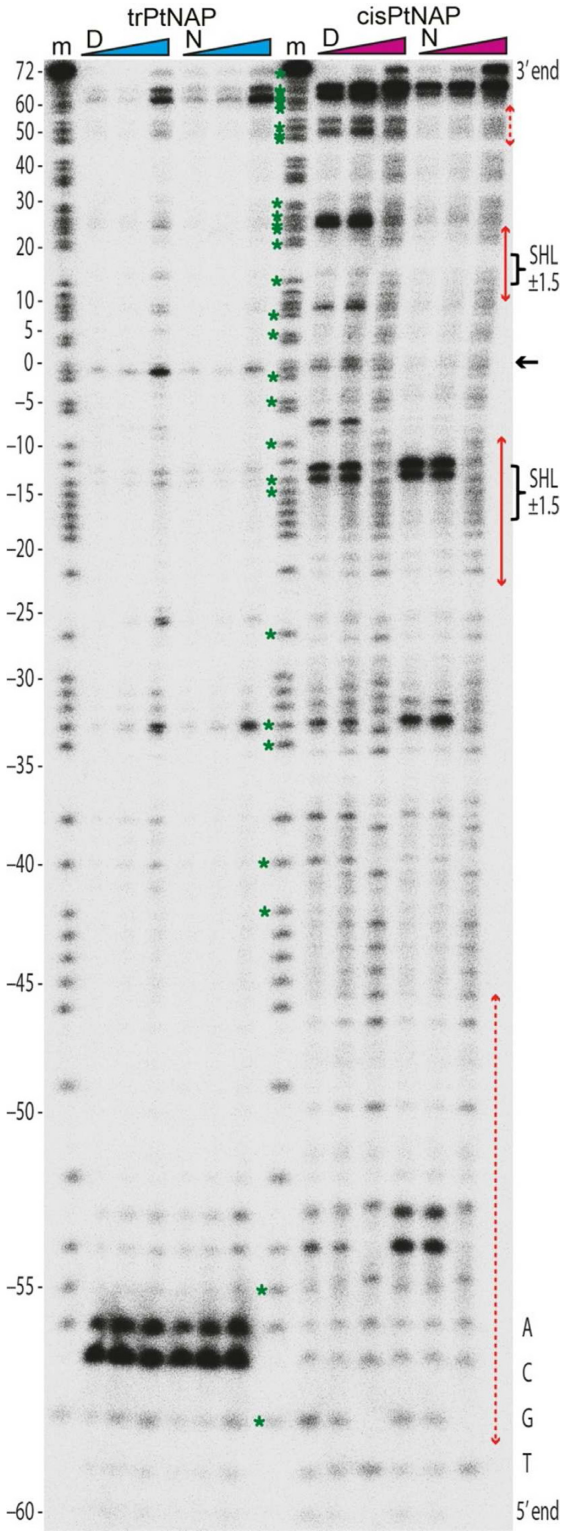

Figure 3. Exonuclease digest analysis shows PtNAP adduct formation profiles. DNA samples, consisting of either NCP (N) or the corresponding naked DNA (D) treated with trPtNAP or cisPtNAP (10-, 20- or 50-fold molar excess of trPtNAP; 5-, 10- or 50-fold molar excess of cisPtNAP), are shown with purine sequencing standards (m). Numbers represent nucleotide position relative to the nucleosome center (black arrow), and green asterisks designate the locations of guanine nucleotides. Red arrows indicate regions of DNA stretching populated in the native NCP crystal structure (solid) and alternative configurations available (dashed).

cal structures between the two symmetry-related sites for a given isomer (Figures 2 and 4, Supplementary Figure S9). This is notable since the DNA conformations in the native state are highly distinct between the regions spanning SHL −1 to −2 and SHL +1 to +2 where the double helix stretching distortions occur in the two symmetry-related halves of the nucleosome. In the 'minus' half, the stretch-associated extreme kink resides at a CA = TG step of SHL −1, whereas due to differences in crystal contacts, the kink instead occurs at the GG = CC step of SHL +1.5 in the 'plus' half of the NCP. In spite of this difference, intercalation is seen to occur in either case within the unstacked GG = CC step, and the resulting DNA conformational parameters are very similar between all the adduct sites. This emphasizes the dynamic nature of exchange between available DNA stretching configurations in the nucleosome, analogous to what we have observed in the past with different DNA attacking agents (16,18,21), but it also indicates that the final conformation resulting from adduct formation by cisPtNAP and trPtNAP is highly constrained. This correspondingly suggests that conformational constraints on reactive intermediates may also be very pronounced, providing a rationale for the site selectivity distinction between these two structural isomers.

Isomer-specific impact on cancer cells

Given the striking distinctions in DNA site selectivity between trPtNAP and cisPtNAP, we conducted experiments on the A2780 tumor cell line to shed more light on how differences in genomic site targeting could influence cellular behaviour. We treated cells with an equal concentration of either agent for 24 h, which apparently yields roughly equivalent genomic DNA adduct levels in the cell, after which we switched cells to agent-free media and quantified cell survival and cell cycle arrest immediately (1-day) and then subsequently 24 and 48 h later (2-day, 3-day; Figure 6, Supplementary Analysis 1–4).

Beyond their general tumor cell growth inhibitory properties, the two compounds display distinct attributes of impact on cell function. In particular, cisPtNAP has much more rapid cancer cell killing activity compared to trPtNAP, with approximately 4-fold more cell death after 1-day exposure to agent (relative to control cells; fraction of dead cells: 12.8% control, 20.3% trPtNAP, 41.0% cisPtNAP). This is consistent with cisPtNAP displaying greater than 11-fold higher cytotoxicity to cancer cells in the short-term (for a 1-day as opposed to the 3-day exposure cell growth inhibition assays; Table 1). Nonetheless, subsequent to removal of free compound from the cell media, exposure to either agent continues to kill a greater fraction of the cell population, and by day 3 the cell death profile of trPtNAP has become similar to that of cisPtNAP. This is also consistent with the fact that the 3-day cytotoxicities of both compounds are very similar.

Given the different rate of cisPtNAP versus trPtNAP tumor cell killing, one would anticipate an analogous differential impact on the cell cycle pattern, but in fact the influence that is observed is in an opposing sense. More specifically, after one day exposure of cancer cells to agent, the degree of cell cycle S-phase arrest (stalling at DNA replication stage)

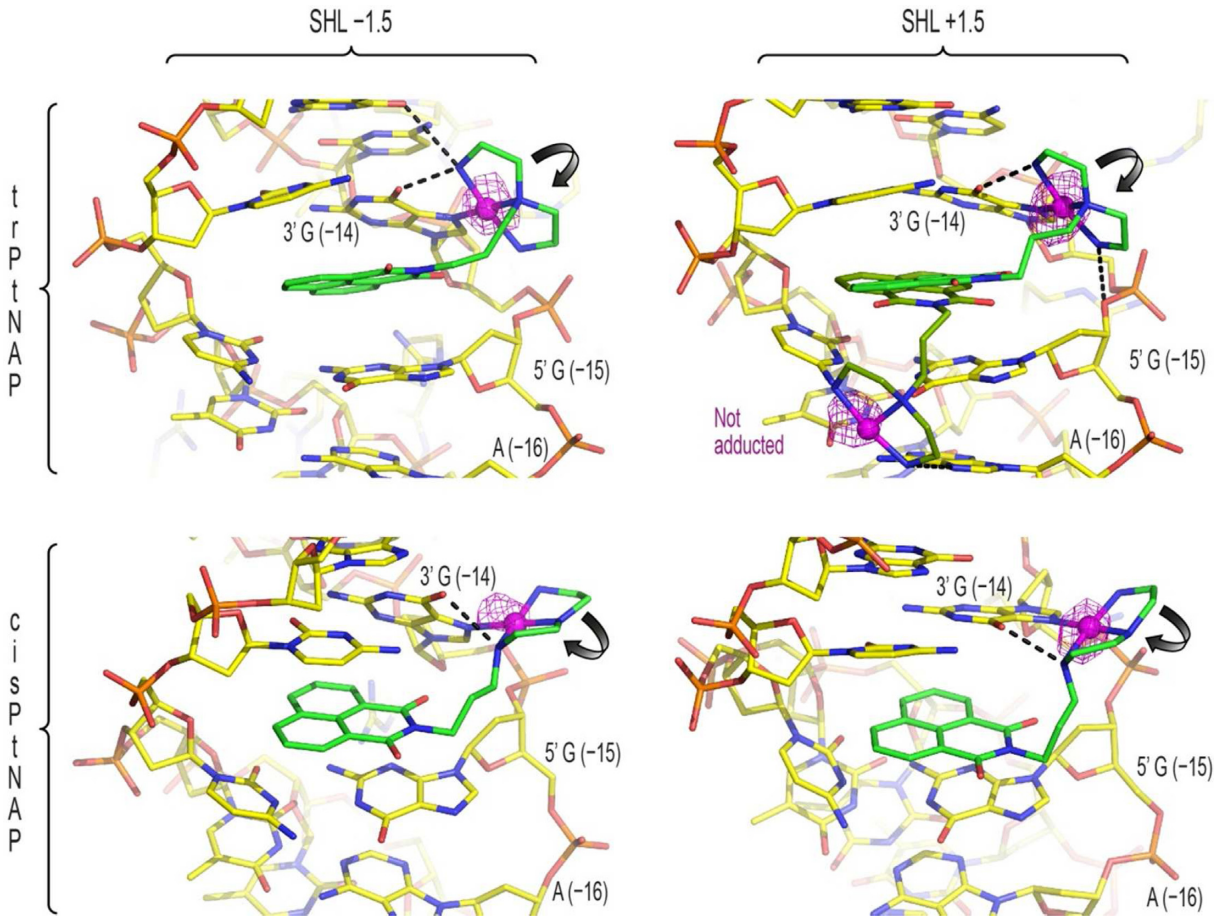

Figure 4. Crystallographic analysis shows trPtNAP and cisPtNAP DNA binding in the nucleosome core. Carbon atoms of the PtNAP ligands are shown in green. Anomalous difference electron density maps appear in magenta (contoured at 9σ, 8σ, 7σ and 10σ for trPtNAP/SHL−1.5, trPtNAP/SHL+1.5, cisPtNAP/SHL−1.5 and cisPtNAP/SHL+1.5, respectively). Hydrogen bonds between ligands and DNA are indicated with dashed lines. Arrows depict rotation of the platinum head group from a putative axially coordinated, pre-reaction, complex to the adducted state, which coincides with the swivel-like rotational freedom of the methylene linker for the cisPtNAP, but not for trPtNAP, intercalated configuration.

induced by trPtNAP is pronounced, but diminishes over the following two days. For cisPtNAP, the degree of S-phase arrest at day 1 is only slight, but then increases by day 3 to a level similar to that seen for trPtNAP at day 1. Moreover, although trPtNAP induces a slight increase in G2/M arrest by day 2, that seen for cisPtNAP is especially pronounced by days 2 and 3.

DISCUSSION

Unlike existing platinum drugs, which form DNA adducts at essentially any solvent exposed guanine bases, whereby steric access is modulated through conformations dictated by DNA sequence and protein binding (18), the compounds we have designed and studied here show striking site selectivity. Although the cisPtNAP adduct formation profile on the naked DNA substrate (in solution) is analogous to what we have observed for platinum drugs, with adducts occurring at many guanine sites, that corresponding to the nucleosomal state is very distinct. Relative to the naked state, most of the guanine sites are rendered unreactive in the NCP, and the only exceptions are the GG dinucleotide sites nearest the 3′ terminus and three other internal locations that display elevated reactivity compared to the naked DNA. These regions within the nucleosome core coincide with adducts forming at dinucleotide sites situated at so-called 'pressure points' of SHL ± 1.5, ± 3.5 and ± 5.5, where the double helix is subjected to the greatest pressure to undergo severe deformation (33,34). This includes foremost kinking into the minor groove, which promotes/allows intercalation at the major groove face of the unstacked bases (16).

The DNA footprinting analysis reveals the superkinked SHL ± 1.5 site to be a hotspot for cisPtNAP adduct formation in the nucleosome core, and this is in excellent agreement with the crystallographic structure of NCP treated with this agent. The double arrest site profile seen in the footprinting indicates adducts at both the 3′ and 5′ guanines of the SHL ± 1.5 GG element, and this is consistent with what is observed in the crystal structure. In fact, the 3′ adduct is more prominent than the 5′ adduct both in the crystallographic as well as the solution data, indicating that the 3′ guanine is more susceptible to attack subsequent to intercalation of the naphthalimide group.

The solution-state adduct formation profile of trPtNAP is fundamentally different than that of cisPtNAP. Whereas

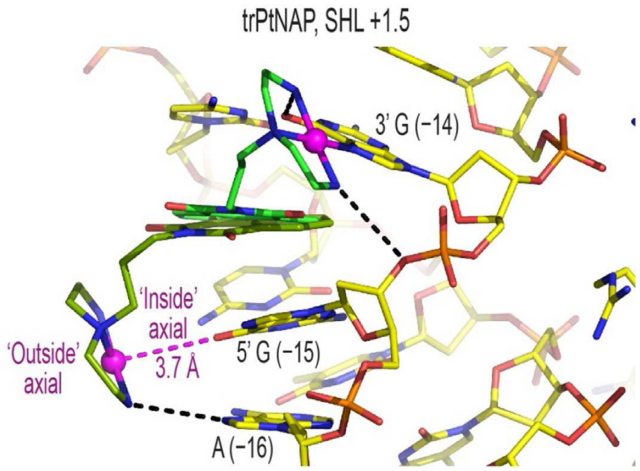

Figure 5. A non-adducted as well as an adducted binding mode is observed for trPtNAP interaction with the nucleosome core. Carbon atoms of the trPtNAP ligands are shown in olive green and bright green for the non-adducted and adducted states, respectively. Hydrogen bonds between ligands and DNA are indicated with black dashed lines. The platinum atom of the non-adducted configuration is situated, along the axial coordination position on the same side ('inside') as the intercalator group, 3.7 Å distant from the O6 atom of guanine −15.

cisPtNAP has no significant avidity to form adduct at the guanine nucleotide nearest the 5′ terminus (−58 G), trPtNAP instead has a pronounced bias to react selectivity at this site. The adduct occurs within a palindromic TGCA element found only at the ends of the DNA. This sequence has been calculated to be amongst the most flexible tetranucleotide elements (35), and within the constraint of containing a reactive G|C dinucleotide would appear to have maximal flexibility by virtue of the flanking CA = TG bp steps, which would correspond to the most flexible guanine-containing dinucleotide type (36).

In spite of the terminal TGCA element having the maximum observed reactivity toward trPtNAP in the solution state (based on the footprinting analysis, Figures 2 and 3), we do not see evidence of adduct formation at this site in the NCP crystal structure. However, intermolecular contacts in the crystal can impose substantial constraints on conformational dynamics, in particular for sites near the DNA termini, which are involved in extensive stacking interactions with neighboring particles. Therefore, it is to be expected that this terminal location does not have the same conformational freedom in the crystalline state as it does in solution. Taken together with the flexibility inherent in the TGCA sequence, this in turn suggests that the adduct formation potential of trPtNAP is strongly dependent on conformational freedom of the double helical substrate.

The trPtNAP adducts that are observed in the NCP structure coincide with 'recognizing' a DNA stretching-induced extreme conformation, which in the native state can fluctuate in form between localizing as a superkink either at SHL ± 1 or SHL ± 1.5. Intercalation is only possible for the SHL ± 1.5 configuration, where the bases are unstacked at the major groove face as opposed to the minor groove face in the case of the SHL ± 1 superkink, but the ability for dynamic interchange between the two conformations allows adduct to accumulate and 'trap' the SHL ± 1.5 deformation (16). However, these deformational substates are likely overall less populated in solution since a greater variety of other states are likely available when the DNA termini are not constrained by crystal contacts. This may explain how the crystalline state would promote SHL ± 1.5 intercalation and allow sufficient residence time for subsequent attack of the platinum group. Nonetheless, a substantial fraction of the trPtNAP seen in the crystal structure is in fact in an unreacted state. This is seen most clearly for the 'plus' nucleosome half where the SHL +1.5 GG dinucleotide is pre-unstacked to allow facile intercalation. Since the electron density profile is inconsistent with the presence of a (electron dense) chloride ion coordinated to the platinum group of the non-adducted trPtNAP (Supplementary Figure S6), the inability of the intercalated agent to fully convert to the adducted state does not appear to stem from a slow rate of aquation. Therefore, the fact that a substantial fraction of the trPtNAP remains in a non-adducted configuration, and additionally considering the 24 h incubation time of the agent with the crystal prior to data collection, indicates that there is a substantial energy barrier associated with reaction at either of the adjacent guanine sites in spite of the proximity afforded by intercalation.

For cisPtNAP, DNA adduct formation is controlled by the intercalation step—sites that are predisposed to intercalation allow reaction to generate adduct subsequent to the non-covalent binding event. In contrast, the reactivity of trPtNAP appears to be largely governed by the stereochemical disposition of the naphthalimide and platinum head groups. In the *cis* configuration, the platinum cycle can swivel between axial and planar DNA-binding modes in line with the dihedral freedom of the methylene linker, providing a favorable reaction pathway through an axially bound transition state (Figure 4, arrows). On the other hand, in the *trans* configuration, the facile direction of platinum head group swivel in line with the freedom of the linker is orthogonal to that which would allow switching between an axial and planar DNA-binding mode. For this reason, in order to form adduct via a pentavalent intermediate associative mechanism, trPtNAP would need to undergo a configurational transition, different from the PtNAP binding modes we see in the crystal structures, which could involve a distinct mode of intercalation, partial de-intercalation or even a non-intercalated state. In fact, the non-covalent trPtNAP binding mode we see at SHL +1.5 shows that orientation of the platinum head group with the 'inside' axial coordination site (facing the linker and naphthalimide group) facing the 5′ guanine base (−15 G) yields a stable, unreactive complex (Figure 5). As such, axial coordination to a guanine-N7 via the 'outside' site (facing opposite linker and naphthalimide group) would appear to require a non-intercalative mode. This may correspondingly rationalize the pronounced sequence preference associated with trPtNAP adduct formation, as likely specific DNA interactions or conformations are effective at promoting the special transition structure(s).

Specific differences in site selectivity between cisPtNAP and trPtNAP notwithstanding, the two compounds display a commonality in having greater DNA site discrimination relative to platinum drugs. Steric constraints afforded by the bimodal nature of the PtNAP agents inhibit

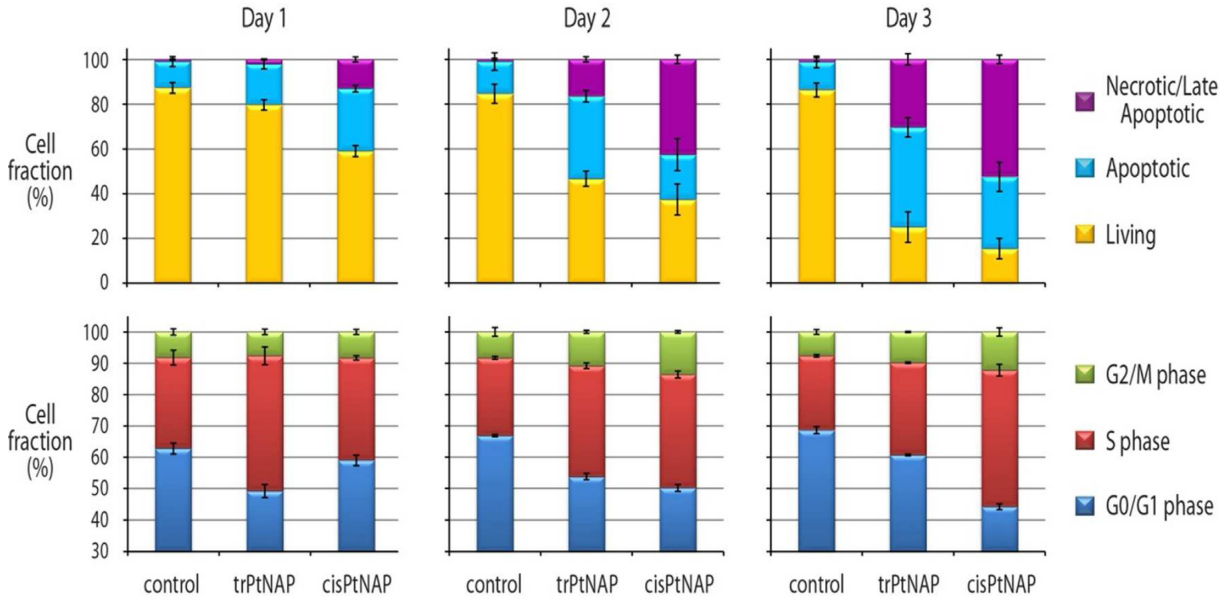

Figure 6. Impact of trPtNAP and cisPtNAP agents on cell viability and function. Apoptosis/necrosis profiles (top) and cell cycle profiles (bottom) were derived from flow cytometric analysis of cultured A2780 cells. Day 1 measurements were made immediately after switching cells to agent-free media (subsequent to 24 h incubation with agent), and Day 2 and Day 3 measurements correspond to cells residing in agent-free media for an additional one or two days (mean ± SD, $n = 3$).

adduct formation at many sites that otherwise coincide with solvent accessible guanine nucleotides. Together with their vastly distinct DNA adduct structures relative to the bifunctional platinum drugs, this may underlie the lack of cross-resistance seen for the PtNAPs toward the cisplatin-resistant tumor cells. Nonetheless, in spite of their higher degree of DNA site discrimination, both compounds generate adducts on genomic DNA more efficaciously than cisplatin (relative to agent concentration). This is consistent with the PtNAPs' greater cytotoxicity toward the ovarian tumor cell line compared to cisplatin, and may also be responsible for their much reduced cytotoxicity toward the more slowly dividing, non-tumorigenic cell line (HaCaT cells) via diminished binding to non-DNA targets.

Considering that the DNA adduct structures as well as cellular DNA adduct formation potential between cisPtNAP and trPtNAP are very similar, their distinct activities on the A2780 cells suggest that differences in where adducts form in the genome may be consequential. However, other possibilities include that additional cellular targets, potentially protein factors, are differentially modified by the two agents. Alternatively, DNA adducts of the two compounds at otherwise the same genomic locations could elicit a distinct impact, for instance in transcription inhibition.

Further investigations will be required to establish whether the differential site selectivity we observe *in vitro* is similar to what occurs within the genome. Nonetheless, the much elevated cytotoxicity of cisPtNAP over trPtNAP in the one-day assays and the distinct ability of cisPtNAP to generate adducts at internal locations within the nucleosome core suggests that such adducts may pose a special challenge to cell survival. As they are known to inhibit DNA repair *in vitro* (11), the internally located adducts may evoke a distinct cellular response that leads to rapid cell death.

The fact that little cell cycle arrest after one-day exposure of cisPtNAP is observed, in spite of extensive cell death, suggests that a population of cells are killed without entering into a (sustained) stalled DNA replication or halted transcriptional status. On the other hand, cells that have survived the initial insult, by day 2 and day 3 (one or two days after compound has been removed from the medium), elicit a substantial degree of S- and G2/M-phase arrest, implying that 'slow' alterations in cell (chromatin) status have occurred that ultimately give rise to replication/transcription arrest. In contrast, adducts formed by trPtNAP instead lead to a distinct process of recognition and response in the short term by causing stalling of DNA replication, apparently thus avoiding cell death, at least temporarily. Moreover, the cell population surviving trPtNAP exposure does not show the long-range cell cycle perturbation seen with cisPtNAP. Since we have recently conducted cell impact analysis of cisplatin (in comparison with ruthenium agents) using the same methodology (21) as for the PtNAPs here, it is interesting to note that the cell cycle arrest profile for cisplatin is more similar to that of trPtNAP. In particular, the S-phase arrest seen for cisplatin and trPtNAP is maximal on day 1 and diminishes sequentially over the following two days. This is a pattern, which is opposite to that of cisPtNAP, suggesting that trPtNAP and cisplatin adducts have an analogous effect on the inhibition of DNA replication.

In the past, defined genomic targets have generally not been considered in the design of metal-based anticancer agents, and yet chromatin affords a multitude of structural and chemical (epigenetic) distinctions that are specific to cellular disposition (6–8). The stereochemically constrained platinum-intercalator compounds we have designed and

studied here, in contrast to current platinum drugs, have a pronounced bias to generate adducts at defined internal nucleosomal sites or at specific DNA sequence elements. Such binding site discrimination would be sensitive to differences in nucleosome positioning, for which there appear to be numerous distinctions between healthy and transformed cells as a consequence of changes to gene expression (6,7,37).

In combination with their favorable antitumor cell and toxicity attributes, cisPtNAP and trPtNAP also display highly distinct influences on cancer cell behaviour, which could translate into differentially exploitable therapeutic profiles. Although many different types of platinum-intercalator species have been studied in the past (38), what we have learned here is that subtle differences in the structure of the compounds can result in very distinct DNA site selectivity. This implies that the precise nature of the intercalator group, the platinum group and the connecting linker can be important in dictating targeting and functional impact. Further studies will be necessary to understand the therapeutic potential of the PtNAPs and related compounds *in vivo* and also to elucidate whether and how differential nucleosome site targeting influences cellular impact. In the future, it may be possible to target genomic sites with metal-based compounds even more specifically—to single out vulnerable points of cancer cells—and the stereochemical principles we have discovered here for tuning adduct formation potential should be helpful in this regard.

ACCESSION NUMBERS

Atomic coordinates and structure factors for the trPtNAP-NCP and cisPtNAP-NCP models have been deposited in the Protein Data Bank under accession codes 4WU8 and 4WU9, respectively.

SUPPLEMENTARY DATA

Supplementary Data are available at NAR Online.

ACKNOWLEDGEMENTS

We thank M. Wang, V. Olieric and staff at the Swiss Light Source (Paul Scherrer Institute, Villigen, Switzerland). Author Contributions: E.Y.D.C. carried out the X-ray crystallographic work and DNA footprinting; G.E.D conducted the cellular assays and quantification of genomic DNA adduct levels; C.F.C. and W.H.A. synthesized cisPtNAP and trPtNAP; P.D. provided expertise on the cellular experiments; C.A.D. designed research, conducted data analysis and wrote the manuscript.

FUNDING

Singapore Ministry of Education Academic Research Fund Tier 2 Programme [19/08]; Ministry of Health National Medical Research Council [NMRC/1312/2011]; Ministry of Education Academic Research Fund Tier 3 Programme [MOE2012-T3–1–001]. Funding for open access charge: Singapore Ministry of Education Academic Research Fund Tier 3 Programme [MOE2012-T3-1-001].
Conflict of interest statement. None declared.

REFERENCES

1. Jung,Y. and Lippard,S.J. (2007) Direct cellular responses to platinum-induced DNA damage. *Chem. Rev.*, **107**, 1387–1407.
2. Todd,R.C. and Lippard,S.J. (2009) Inhibition of transcription by platinum antitumor compounds. *Metallomics*, **1**, 280–291.
3. Kelland,L. (2007) The resurgence of platinum-based cancer chemotherapy. *Nat. Rev. Cancer*, **7**, 573–584.
4. Rabik,C.A. and Dolan,M.E. (2007) Molecular mechanisms of resistance and toxicity associated with platinating agents. *Cancer Treat. Rev.*, **33**, 9–23.
5. Davey,G.E. and Davey,C.A. (2008) Chromatin—a new, old drug target? *Chem. Biol. Drug Des.*, **72**, 165–170.
6. Baylin,S.B. and Jones,P.A. (2011) A decade of exploring the cancer epigenome—biological and translational implications. *Nat. Rev. Cancer*, **11**, 726–734.
7. Rodriguez-Paredes,M. and Esteller,M. (2011) Cancer epigenetics reaches mainstream oncology. *Nat. Med.*, **17**, 330–339.
8. Sharma,S.V., Lee,D.Y., Li,B., Quinlan,M.P., Takahashi,F., Maheswaran,S., McDermott,U., Azizian,N., Zou,L., Fischbach,M.A. *et al.* (2010) A chromatin-mediated reversible drug-tolerant state in cancer cell subpopulations. *Cell*, **141**, 69–80.
9. Silva,J.M., Marran,K., Parker,J.S., Silva,J., Golding,M., Schlabach,M.R., Elledge,S.J., Hannon,G.J. and Chang,K. (2008) Profiling essential genes in human mammary cells by multiplex RNAi screening. *Science*, **319**, 617–620.
10. Schlabach,M.R., Luo,J., Solimini,N.L., Hu,G., Xu,Q., Li,M.Z., Zhao,Z., Smogorzewska,A., Sowa,M.E., Ang,X.L. *et al.* (2008) Cancer proliferation gene discovery through functional genomics. *Science*, **319**, 620–624.
11. Wang,D., Hara,R., Singh,G., Sancar,A. and Lippard,S.J. (2003) Nucleotide excision repair from site-specifically platinum-modified nucleosomes. *Biochemistry*, **42**, 6747–6753.
12. Ong,M.S., Richmond,T.J. and Davey,C.A. (2007) DNA stretching and extreme kinking in the nucleosome core. *J. Mol. Biol.*, **368**, 1067–1074.
13. Wu,B., Mohideen,K., Vasudevan,D. and Davey,C.A. (2010) Structural insight into the sequence dependence of nucleosome positioning. *Structure*, **18**, 528–536.
14. Pryciak,P.M. and Varmus,H.E. (1992) Nucleosomes, DNA-binding proteins, and DNA sequence modulate retroviral integration target site selection. *Cell*, **69**, 769–780.
15. Pruss,D., Bushman,F.D. and Wolffe,A.P. (1994) Human immunodeficiency virus integrase directs integration to sites of severe DNA distortion within the nucleosome core. *Proc. Natl. Acad. Sci. U.S.A.*, **91**, 5913–5917.
16. Davey,G.E., Wu,B., Dong,Y., Surana,U. and Davey,C.A. (2010) DNA stretching in the nucleosome facilitates alkylation by an intercalating antitumour agent. *Nucleic Acids Res.*, **38**, 2081–2088.
17. Wu,B., Droge,P. and Davey,C.A. (2008) Site selectivity of platinum anticancer therapeutics. *Nat. Chem. Biol.*, **4**, 110–112.
18. Wu,B., Davey,G.E., Nazarov,A.A., Dyson,P.J. and Davey,C.A. (2011) Specific DNA structural attributes modulate platinum anticancer drug site selection and cross-link generation. *Nucleic Acids Res.*, **39**, 8200–8212.
19. Hossain,S.U., Sengupta,S. and Bhattacharya,S. (2005) Synthesis and evaluation of antioxidative properties of a series of organoselenium compounds. *Bioorg. Med. Chem.*, **13**, 5750–5758.
20. Mahalanobis,P.C. (1936) On the generalised distance in statistics. *Proc. Natl. Inst. Sci. India*, **2**, 49–55.
21. Adhireksan,Z., Davey,G.E., Campomanes,P., Groessl,M., Clavel,C.M., Yu,H.J., Nazarov,A.A., Yeo,C.H.F., Ang,W.H., Droge,P. *et al.* (2014) Ligand substitutions between ruthenium-cymene compounds can control protein versus DNA targeting and anticancer activity. *Nat. Commun.*, **5**, 3462.
22. Maxam,A.M. and Gilbert,W. (1980) Sequencing end-labeled DNA with base-specific chemical cleavages. *Meth. Enzymol.*, **65**, 499–560.
23. Davey,C.A., Sargent,D.F., Luger,K., Maeder,A.W. and Richmond,T.J. (2002) Solvent mediated interactions in the structure of the nucleosome core particle at 1.9 Å resolution. *J. Mol. Biol.*, **319**, 1097–1113.
24. Wu,B., Ong,M.S., Groessl,M., Adhireksan,Z., Hartinger,C.G., Dyson,P.J. and Davey,C.A. (2011) A ruthenium antimetastasis agent

forms specific histone protein adducts in the nucleosome core. *Chemistry*, **17**, 3562–3566.
25. Leslie,A.G. (2006) The integration of macromolecular diffraction data. *Acta Crystallogr. D Biol. Crystallogr.*, **62**, 48–57.
26. Bailey,S. (1994) The CCP4 suite: programs for protein crystallography. *Acta Crystallogr. D Biol. Crystallogr.*, **50**, 760–763.
27. Vasudevan,D., Chua,E.Y. and Davey,C.A. (2010) Crystal structures of nucleosome core particles containing the '601' strong positioning sequence. *J. Mol. Biol.*, **403**, 1–10.
28. Ndinguri,M.W., Fronczek,F.R., Marzilli,P.A., Crowe,W.E., Hammer,R.P. and Marzilli,L.G. (2010) Exploring water-soluble Pt(II) complexes of diethylenetriamine derivatives functionalized at the central nitrogen. Synthesis, characterization, and reaction with 5 '-GMP. *Inorg. Chim. Acta*, **363**, 1796–1804.
29. Lu,X.J. and Olson,W.K. (2003) 3DNA: a software package for the analysis, rebuilding and visualization of three-dimensional nucleic acid structures. *Nucleic Acids Res.*, **31**, 5108–5121.
30. Zheng,G., Lu,X.J. and Olson,W.K. (2009) Web 3DNA–a web server for the analysis, reconstruction, and visualization of three-dimensional nucleic-acid structures. *Nucleic Acids Res.*, **37**, W240–W246.
31. Behrens,B.C., Hamilton,T.C., Masuda,H., Grotzinger,K.R., Whang-Peng,J., Louie,K.G., Knutsen,T., McKoy,W.M., Young,R.C. and Ozols,R.F. (1987) Characterization of a cis-diamminedichloroplatinum(II)-resistant human ovarian cancer cell line and its use in evaluation of platinum analogues. *Cancer Res.*, **47**, 414–418.
32. Dyer,P.N., Edayathumangalam,R.S., White,C.L., Bao,Y., Chakravarthy,S., Muthurajan,U.M. and Luger,K. (2004) Reconstitution of nucleosome core particles from recombinant histones and DNA. *Methods Enzymol.*, **375**, 23–44.
33. Richmond,T.J. and Davey,C.A. (2003) The structure of DNA in the nucleosome core. *Nature*, **423**, 145–150.
34. Chua,E.Y., Vasudevan,D., Davey,G.E., Wu,B. and Davey,C.A. (2012) The mechanics behind DNA sequence-dependent properties of the nucleosome. *Nucleic Acids Res.*, **40**, 6338–6352.
35. Packer,M.J., Dauncey,M.P. and Hunter,C.A. (2000) Sequence-dependent DNA structure: Tetranucleotide conformational maps. *J. Mol. Biol.*, **295**, 85–103.
36. Krueger,A., Protozanova,E. and Frank-Kamenetskii,M.D. (2006) Sequence-dependent basepair opening in DNA double helix. *Biophys. J.*, **90**, 3091–3099.
37. Lin,J.C., Jeong,S., Liang,G., Takai,D., Fatemi,M., Tsai,Y.C., Egger,G., Gal-Yam,E.N. and Jones,P.A. (2007) Role of nucleosornal occupancy in the epigenetic silencing of the MLH1 CpG island. *Cancer Cell*, **12**, 432–444.
38. Baruah,H., Barry,C.G. and Bierbach,U. (2004) Platinum-intercalator conjugates: from DNA-targeted cisplatin derivatives to adenine binding complexes as potential modulators of gene regulation. *Curr. Top. Med. Chem.*, **4**, 1537–1549.